Biogeosciences

Modeling pCO_2 Variability in the Gulf of Mexico

Zuo (George) Xue[1, 2, &3], Ruoying He[4], Katja Fennel[5], Wei-Jun Cai[6], Steven Lohrenz[7], Wen-Jen Huang[8]， Hanqin Tian[9], Wei Ren[10], Zhengchen Zang[1]

1. Dept. of Oceanography and Coastal Sciences, Louisiana State University, Baton Rouge, LA, United States
2. Center for Computation and Technology, Louisiana State University, Baton Rouge, LA, United States
3. Coastal Studies Institute, Louisiana State University, Baton Rouge, LA, United States
4. Dept. of Marine, Earth & Atmospheric Sciences, North Carolina State University, Raleigh, NC, United States
5. Dept. of Oceanography, Dalhousie University, Halifax, Canada
6. School of Marine Science and Policy, University of Delaware, Newark, DE, United States
7. School for Marine Science and Technology, University of Massachusetts Dartmouth, New Bedford, MA, United States
8. Department of Oceanography, National Sun Yat-sen University, Kaohsiung, Taiwan
9. School of Forestry and Wildlife Sciences, Auburn University, AL, United States
10. Department of Plant and Soil Sciences, University of Kentucky, Lexington, KY, United States

Abstract

A three-dimensional coupled physical-biogeochemical model was used to simulate and quantify temporal and spatial variability of sea surface pCO_2 in the Gulf of Mexico (GoM). The model was driven by realistic atmospheric forcing, open boundary conditions from a data-assimilative global ocean circulation model, and observed freshwater and terrestrial nutrient and carbon input from major rivers. A seven-year model hindcast (2004–2010) was performed and validated against ship measurements. Model results revealed clear seasonality in surface pCO_2 and were used to compute carbon budgets in the Gulf. On average, the GoM was found to be a CO_2 sink with a flux of $1.11 \pm 0.84 \times 10^{12}$ mol C yr^{-1}, which, together with the enormous fluvial carbon input, was balanced by the carbon export through the Loop Current. Two model sensitivity experiments were performed: one without biological sources and sinks and the other using river input from the 1904-1910 period as simulated by the Dynamic Terrestrial Ecosystem Model (DLEM). It was found that biological uptake was the primary driver making GoM an overall CO_2 sink and that the sub-regional carbon budget was susceptible to changes in river forcing. When the 1904-1910 river conditions were applied, the northern GoM became a CO_2 source instead.

1. Introduction

Human consumption of fossil fuels has resulted in continuously increasing levels of atmospheric CO_2 since the Industrial Revolution began around 1750. If the increasing trend continues, the projected pCO_2 by the end of the 21st century (970 ppm, in A1F1 scenario, Stocker et al., 2014) could be nearly triple the present level. In the face of different climate scenarios, a better understanding of the oceans' role in regulating the global carbon cycle is crucial, because oceans not only act as receivers of the enormous carbon loading from coastal rivers (Cai et al., 2011a; Bauer et al. 2013), but also as vast carbon reservoirs via the "carbon pump" mechanism (Sabine et al., 2004; Sabine and Tanhua, 2010). On regional scales, the marine carbon cycle tends to be more complicated and shows contrasting behaviors in different areas (coastal vs. open ocean, low latitude vs. high latitude, etc.) and during different seasons (e.g., Lohrenz et al., 2010 for the northern Gulf of Mexico; Jiang et al., 2008 for the South Atlantic Bight; Signorini et al., 2013 for the North American east coast; Tsunogai et al., 1999 for the East China Sea). Quantifying the ocean carbon budget is therefore a difficult task. Coupled physical and biological models are useful tools for understanding complex biogeochemical processes and estimating carbon and nutrient fluxes in coastal oceans where spatial and temporal heterogeneities are high and data are sparse (e.g. Fennel and Wilkin, 2009; Fennel 2010; Fennel et al., 2011; and He et al., 2011).

Our study focuses on the carbon cycle in the Gulf of Mexico (GoM). One unique feature of the Gulf is that it receives enormous riverine nutrient and carbon inputs, both organic and inorganic, the majority of which are from the Mississippi-Atchafalaya River system. Excessive nutrient loading causes coastal eutrophication, which triggers not only

63 the well-known hypoxia phenomenon (a.k.a. the "Dead Zone", Rabalais et al., 2002), but
64 also a newly revealed coastal ocean acidification problem (Cai et al, 2011b). However,
65 the carbon budget associated with such enormous terrestrial carbon and nutrient inputs
66 remains unclear: on the one hand extensive riverine carbon input results in CO_2 over-
67 saturation in coastal waters, which serve as a CO_2 source to the atmosphere (e.g. Lohrenz
68 et al., 2010; Guo et al., 2012); on the other hand, although the Mississippi River Plume
69 region is an overall heterotrophic system that breaks down organic carbon (Murrell et al.,
70 2013), enhanced primary production in the river plume due to significant inputs of
71 inorganic nutrients induces a net influx of CO_2. Further offshore, the circulation in the
72 GoM is largely influenced by the energetic Loop Current. Large anticyclonic eddies
73 aperiodically pinch off from the Loop Current (Sturges and Leben, 2000), which, along
74 with the wind-driven cross-shelf circulation and other meso-scale and sub-mesoscale
75 processes, enhance material exchanges between the eutrophic coastal waters and
76 oligotrophic deep-ocean waters (e.g., Toner et al., 2003). Indeed, a recent observational
77 study suggested a significant dissolved inorganic carbon export (DIC, ~ 3.30×10^{12} mol
78 C yr^{-1}) from the GoM shelves to the Loop Current waters (Wang et al., 2013).
79 While global inorganic carbon budgets have been made available through joint
80 seawater CO_2 observations (e.g. World Ocean Circulation Experiment and Joint Global
81 Ocean Flux study, Sabine et al., 2004; Feely et al., 2004; Orr et al., 2005), they are too
82 coarse to represent CO_2 variability in the GoM (Gledhill et al., 2008). Other recent efforts
83 were able to provide GoM sub-regional carbon assessments based on limited in situ
84 observations (e.g. Cai et al., 2003, Lohrenz et al., 2010, Huang et al., 2013, 2015a and
85 2015b focused on the Mississippi River plume and the Louisiana Shelf; Wang et al., 2013

86 covered three cross-shelf transects in the northeastern GoM but only for one summer).
87 Significant uncertainties exist in such budget estimations due to large temporal and
88 spatial gaps presented in the observations (e.g. Coble et al., 2010; Hofmann et al., 2011;
89 Robbins et al., 2014). In this regard, coupled physical-biogeochemical models are
90 capable of representing the biogeochemical cycle with realistic physical settings (e.g.,
91 ocean mixing and advection) and providing an alternative means for a Gulf-wide carbon
92 budget assessment.

93 Here we present a GoM pCO_2 analysis based on the results of a coupled physical-
94 biogeochemical model simulation. Our objective is to quantify the CO_2 flux at the air-sea
95 interface (which at present is based on observational analyses alone and subject to large
96 uncertainty), as well as its variability in relationship with river plume dynamics and
97 dominant oceanic processes in different regions of the GoM.

98

99 **2. Method**

100 Our analysis uses solutions from a coupled physical-biogeochemical model
101 covering the GoM and South Atlantic Bight waters (Xue et al., 2013, model domain see
102 Fig.1). The circulation component of the coupled model is the Regional Ocean Modeling
103 System (ROMS, Haidvogel et al. 2008, Shchepetkin and McWilliams, 2005; Hyun and
104 He, 2010) and is coupled with the biogeochemical module described in Fennel et al.
105 (2006, 2008, and 2011). The nitrogen cycling parameterization has seven state variables:
106 two species of dissolved inorganic nitrogen (DIN hereafter, nitrate [NO_3] and ammonium
107 [NH_4]), one functional phytoplankton group, chlorophyll as a separate state variable to
108 allow for photoacclimation, one functional zooplankton group, and two pools of detritus

representing large, fast-sinking particles, and suspended, small particles. The carbon cycle is connected to the nitrogen cycle via a C to N ratio of 6.625 for the organic components (phytoplankton, zooplankton, large and small detritus). The sediment component of the biogeochemical model is a simplified representation of benthic remineralization processes, where the flux of sinking organic matter out of the bottommost grid box results immediately in a corresponding influx of ammonium and DIC at the sediment/water interface. The parameterization accounts for the loss of fixed nitrogen through sediment denitrification based on the linear relationship between sediment oxygen consumption and denitrification reported by Seitzinger and Giblin (1996) and only accounts for the portion of denitrification that is supported by nitrification of ammonium in the sediment (referred to as coupled nitrification/denitrification.

A seven-year (January 1, 2004–December 31, 2010) model hindcast was performed, driven by NCEP's high resolution combined model and assimilated atmospheric dataset (North American Regional Reanalysis, www.cdc.noaa.gov), open boundary conditions for ocean model (temperature, salinity, water level, and velocity) from a data-assimilative global ocean circulation model (HYCOM/NCODA, Chassignet et al., 2007), and observed freshwater and terrestrial nutrient input from 63 major rivers (Aulenbach et al., 2007; Milliman and Farnsworth, 2011; Fuentes-Yaco et al., 2001; and Nixon, 1996). Model validations (physics, nutrients and chlorophyll) and a nitrogen budget were reported in Xue et al. (2013).

In this study, we have focused on the carbon cycle in the GoM. As in Xue et al. (2013), we considered the first year of the simulation (2004) as model spin-up; all results

132 presented here use model output from 2005 to 2010. The carbonate chemistry of the
133 coupled model is based on the standard defined by the Ocean Carbon Cycle Model
134 Intercomparison Project Phase 2 (Orr et al., 2000). There are two active tracers, DIC and
135 alkalinity, to determine the other four variables of the carbonate system (i.e. pCO_2,
136 carbonate ion concentration, bicarbonate ion concentration, and pH; Zeebe and Wolf-
137 Gladrow, 2001). Details of the formulas used in the simulation are provided in the
138 supplementary materials S1.

139 Similar to the results reported by Hofmann et al. (2011), we found that the model-
140 simulated DIC concentration in the water column was very sensitive to the initial
141 conditions. Although there are many historical measurements in the GoM, these data are
142 limited to the northern GoM shelf regions and thus are insufficient to initialize the model.
143 Instead, we tested model sensitivity using three sets of initial and open boundary
144 conditions, which were derived using the empirical salinity-temperature-DIC-alkalinity
145 relationships described in Lee et al. (2000 and 2006), Cai et al. (2011a), and Wang et al.
146 (2013), respectively. Among them, the initial condition prescribed following Lee et al.
147 (2000 and 2006, Fig.2, details see supplementary materials S2) provided the best model-
148 data comparison. For the open boundary condition, we found simulated surface pCO_2
149 exhibited very limited variance (<5%) regardless of which conditions were applied. To be
150 consistent with the setup of the initial condition, the results presented here were driven by
151 boundary conditions derived from Lee et al., (2000 and 2006). For particular organic
152 carbon, we set a small, positive value for both phytoplankton and zooplankton along the
153 open boundaries.

The carbon cycle parameterizations used in this study followed the same approach and values as in Fennel et al. (2008), Fennel and Wilkin (2009), and Fennel (2010). For gas exchange calculations we followed the formulas in Wanninkhof (1992, details see supplementary materials S3). For air pCO_2, we utilized the Atmospheric Infrared Sounder (AIRS, 2008) monthly gridded observation dataset and averaged them over the study area. We applied the curve-fitting method using a C language program named CCGCRV (http://www.esrl.noaa.gov/gmd/ccgg/mbl/crvfit/crvfit.html, Fig.3), and the air pCO_2 in the gas exchange calculation was prescribed as:

$$pCO_{2air} = D0 + D1*t + D2*(t^2) + D3*\sin(pi2*t) + D4*\cos(pi2*t) + D5*\sin(pi2*2*t) + D6*\cos(pi2*2*t) \quad (1)$$

where pCO_{2air} represents the monthly air pCO_2; t represents the number of months since January 2004 divided by 12, $pi2$ is a constant set to 6.28, $D0$=375.96, $D1$=2.23, $D2$=-0.007, $D3$=1.31, $D4$=-0.64, $D5$= -0.13, $D6$=0.21, and $D7$=0.09. Due to the relatively low horizontal resolution of the AIRS data (2.5*2 degree), air pCO_2 was set to be spatially uniform.

To account for riverine inputs, we constructed climatological monthly alkalinity time series by averaging all available U.S. Geological Survey (USGS) observations for each major river, including the Mississippi, Atchafalaya, Mobile, and Brazos in the GoM. Because direct riverine DIC measurements were not available, we approximated riverine DIC inputs using the corresponding alkalinity value plus 50, following the observational study by Guo et al. (2012). The fluvial DIC input to the GoM was estimated as ~ 2.18 ×

176 10^{12} mol C yr^{-1}, the majority of which was delivered by the Mississippi-Atchafalaya
177 River (~ 1.80×10^{12} mol C yr^{-1}, Fig.4, comparable with the estimation in Cai et al., 2003).
178 The results of three model experiments covering the period of 2004-2010 are
179 presented in this study, in which, Experiment 1 (Exp1) was a "control run", with
180 observed riverine inputs from USGS and biological sources and sinks of DIC and
181 alkalinity in the water column; Experiment 2 (Exp2) was a "no-biology run", where all
182 biological sources and sinks of DIC and alkalinity were disabled, similar to the
183 experiment described in Fennel and Wilkin (2009); and Experiment 3 (Exp3) had the
184 same set up as Exp1, but the riverine inputs (water, nutrients, and carbon of the
185 Mississippi-Atchafalaya river) were taken from the Dynamic Land Ecosystem Model
186 (DLEM, Tian et al., 2015) simulation for the period of 1904-1910 (Fig. 4). Specifically,
187 we used the monthly model outputs of water, NO_3, NH_4, and alkalinity from DLEM as
188 riverine inputs to drive the ocean model in Exp1. Also in Exp3 the air pCO_2 was set to
189 the 1904-1910 condition derived by formula (1). The purpose of Exp2 was to examine
190 the role of biological processes in regulating regional pCO_2 variability, whereas Exp3
191 examined connections between variability of coastal carbon dynamics and historical
192 climate (the first ten years of the 20^{th} century vs. that of the 21^{st} century) and land-use
193 changes within the Mississippi watershed.
194
195 **3. Validation of the control run**
196 We utilized the ship-based sea surface pCO_2 database compiled by the Lamont-
197 Doherty Earth Observatory (LDEO Version 2014, >180,000 data points in the Gulf over
198 2005-2010, Takahashi et al., 2015) and Huang et al. (2015a and b) for model validation

199 (see locations of ship measurements in Fig.5). The ship measurements by Huang et al.
200 (2015a and b) were taken in October 2005; April, June, August 2006; May, August 2007;
201 January, April, July, November 2009; and March 2010, respectively and contain > 78,000
202 data points. To alleviate the spatial and temporal mismatches associated with these in-situ
203 measurements, we computed their temporal and spatial mean using a 10-day temporal
204 binning for temporal processing, and then compared them with model-simulated pCO_2
205 time series (Fig.6). To facilitate our analysis, the GoM was divided into five sub-regions:
206 1) Mexico Shelf (MX Shelf), 2) West Gulf of Mexico Shelf (WGoM Shelf), 3) Northern
207 Gulf of Mexico Shelf (NGoM Shelf), 4) West Florida Shelf (WF Shelf), and 5) the open
208 ocean, which is > 200m water depth (regional definitions followed Benway and Coble,
209 2014, maps of sub-regions see Fig.1). The data points falling in each of the sub-regions
210 was first grouped by a 10-day temporal binning and then spatially averaged to get a mean
211 value for each sub-region.

212 On the NGoM Shelf, the control simulation was able to capture the measured
213 pCO_2 in 21 out of the 26 data groups (the mean value of in-situ measurements fell within
214 one standard deviation of the model mean). Specifically, agreement between model and
215 observations was better during spring, fall, and winter, than during summer. The model
216 overestimated pCO_2 in June 2006, August 2007, and July 2009. These discrepancies will
217 be discussed in later sections. On the Gulf-wide scale, the control run reproduced the
218 observed seasonality. Decent model-data agreements were found in 24 out of the 26 data
219 groups. These sub-regional and Gulf-wide comparisons indicate that the coupled
220 physical-biogeochemical model is generally capable of resolving temporal and spatial

variations in observed pCO_2, allowing us to use this seven-year hindcast to further characterize the air-sea CO_2 flux.

4. Results

In this section, we present model-simulated sea surface pCO_2 and air-sea CO_2 flux in the five sub-regions. Because large pCO_2 gradients were found in both in-situ measurements and model simulation in shallow waters, areas that are shallower than 10 m were excluded from our analysis.

4.1 Temporal variability of Sea Surface pCO_2

Spatially averaged model-simulated pCO_2 on the NGoM Shelf exhibited clear seasonality, with large values (~ 500 ppm) around August and smallest values (~ 300 ppm) around February (Fig.6a). Notably, spatially averaged pCO_2 on the NGoM Shelf was not coincident with high river carbon and nutrient inputs (Fig.3). Peaks in pCO_2 were generally simulated two to three months later than the annual maximum in river input. The maximum riverine input during 2005-2010 was observed in June 2008 when a major flood occurred (Fig. 4a), yet no significant elevation of pCO_2 was seen in the model simulation. Gulf-wide spatially averaged pCO_2 (Fig.4b) had a temporal pattern similar to that on the NGoM Shelf, with high pCO_2 values (~ 425 ppm) in August and low values (~ 350 ppm) in February. Averaged pCO_2 on the NGoM Shelf was generally 50 ppm higher than that in the entire Gulf.

244 **4.2 Air-Sea CO_2 flux**

245 The carbon flux was calculated from a multi-year model mean (2005-2010). We
246 found that the GoM overall was a CO_2 sink with a mean flux rate of 0.71±0.54 mol C m^{-2}
247 yr^{-1} (~ 1.11±0.84 × 10^{12} mol C yr^{-1}, Table 1 and Fig.7). Examining region by region, we
248 found that the open ocean, occupying ~ 65% of the GoM by area, acted as a CO_2 sink
249 (1.04±0.46 mol m^{-2} yr^{-1} of C) during most of the year except in summer. The greatest
250 carbon uptake occurred in winter (2.44±0.49 mol C m^{-2} yr^{-1}). It is evident that waters
251 around the Loop Current act as a sink throughout the year, whereas the western part of
252 the open ocean waters shifted from acting as a CO_2 source in summer and fall to a sink in
253 winter and spring.

254 Compared with the open ocean, air-sea flux on the continental shelf was more
255 location-dependent and varied from season to season. Among the four shelf sub-regions,
256 the MX Shelf has the largest area. It acted as a strong CO_2 sink in winter and spring
257 (0.49±0.28 and 0.97±0.28 mol C m^{-2} yr^{-1}) and then a carbon source in summer and fall (-
258 0.96±0.38 and -0.76±0.45 mol C m^{-2} yr^{-1}). Waters along the eastern side of the MX Shelf
259 were a sink during most of the year, while to the west the shelf was a source in summer
260 and fall. On an annual scale, this region was a sink with an air-sea flux of 0.19±0.35 mol
261 C m^{-2} yr^{-1}. To the north, the WGoM Shelf has the smallest area among the four shelf sub-
262 regions. It acted as a CO_2 source during spring, summer, and fall (-0.24±0.59, -1.69±0.43
263 and -1.06±0.34 mol C m^{-2} yr^{-1}) and a strong CO_2 sink during winter (1.62±0.32 mol C m^{-2}
264 yr^{-1}). On an annual scale the WGoM region was a CO_2 source with a degassing rate of
265 0.34±0.42 mol C m^{-2} yr^{-1}.

The NGoM Shelf shifted from acting as a CO_2 source in summer and fall (-1.42±0.74 and -0.79±0.63 mol C m^{-2} yr^{-1}) to a sink in winter and spring (1.01±0.89 and 2.49±0.70 mol C m^{-2} yr^{-1}). The most prominent feature here was the continuous, strong degassing in the coastal waters around the Mississippi-Atchafalaya River mouths. However, as the water becomes deeper, the NGoM Shelf water shifted from acting as a sink during winter and spring to a source during summer and fall. Despite of the extensive degassing in the coastal water, the NGoM Shelf overall was a CO_2 sink on a yearly basis (0.32±0.74 mol C m^{-2} yr^{-1}). Similarly, the WF Shelf also shifted from acting as a CO_2 source in summer and fall (-1.26±0.53 and -1.73±0.67 mol C m^{-2} yr^{-1}) to a sink in winter and spring (1.19±0.38 and 0.28±0.33 mol C m^{-2} yr^{-1}). The degassing in the inner shelf was strong enough to make the WF Shelf a CO_2 source on a yearly basis (-0.38±0.48 mol C m^{-2} yr^{-1}).

Despite the salient spatial and temporal variability, the GoM was an overall CO_2 sink, mainly because of the strong uptake in the open ocean. For validation purposes, we compared (in Table 1) model-simulated air-sea flux against an estimation based on observations, which utilized all available measurements collected within the GoM from 2005 to 2010 (Robbins et al., 2014). Our control-run estimations generally agree with in-situ measurements in all five sub-regions in terms of the ocean's role as a CO_2 source or sink. There is some discrepancy in the magnitude of the estimated flux, specifically in the Open Ocean sub-region. We note that Robbins et al. (2014) used monthly mean pCO_2 and wind fields in their calculation as opposed to the 10-day interval we used here. Therefore, to facilitate the comparison of results, we recalculated the flux using a monthly mean pCO_2 and wind fields and obtained a flux estimate of 0.31±0.35 mol C m^{-2}

289 yr^{-1} for the Open Ocean sub-region, and 0.12±0.23 mol C m^{-2} yr^{-1} for the entire GoM.
290 These values are comparable to those in Robbins et al. (2014, 0.48±0.07 mol C m^{-2} yr^{-1}
291 for the Open Ocean and 0.19±0.08 mol C m^{-2} yr^{-1} for the entire GoM).
292
293 **4.3 Net Community Production**
294 As Net Community Production (NCP) plays an important role in regulating water
295 CO_2 concentration, we generated maps of seasonal mean surface NCP as well as time
296 series of spatially averaged surface NCP for the NGoM and Open Ocean in Figs. 8 and 9.
297 High NCP was simulated in the surface NGoM water and near the eastern tip of the MX
298 shelf for of the year. For the NGoM shelf, surface NCP peaks in the late spring and early
299 summer, with the highest value (2.62 mmol N/m^3) simulated in summer 2008 when there
300 was a major flooding event. Compared with the NGoM condition (0.53 mmol N/m^3),
301 mean surface NCP in the Open Ocean was relatively small, with a multi-year mean value
302 of 0.11 mmol N/m^3. In addition, the Gulf-wide mean surface NCP exhibited peaks in late
303 winter and early spring, mainly incurred by the strong upwelling along the west side of
304 the Yucatan Strait (Figs. 8a and 8d). Compared with the surface NCP, bottom NCP was
305 found to be small (0.05 mmol N/m^3 for the NGoM) and is thus not shown.
306
307 **4.4 Model Sensitivity experiments: No-biology simulation (Exp2)**
308 To test the role of biological processes in regional CO_2 variability, a no-biology
309 run was conducted, where all biology sources and sinks of DIC and alkalinity were
310 disabled similar to the experiment described in Fennel and Wilkin (2009). The
311 experiment produced higher surface pCO_2 than the control run. $pCO2$ is strongly elevated

312 around the Mississippi River Delta on the NGoM shelf during spring and summer. For
313 the Open Ocean, the pCO_2 increase was mainly confined within the loop current and was
314 strongly impacted by Caribbean waters flowing in through the Yucatan Channel (Fig. 10).
315 To assess the influence of NCP on CO_2 variation, we plotted the pCO_2 difference between
316 the Control run (Exp1) and No-biology run (Exp2) against the surface NCP from the
317 Control run in Fig. 11. In the NGoM, the pCO_2 difference between the Control run and
318 No-biology run was strongly correlated with NCP (r=0.80), indicating a regional
319 biological carbon removal For the Open Ocean, the pCO_2 difference shows no correlation
320 with NCP, and we speculate that the biological carbon removal in this region was
321 incurred not only by local NCP, but also remote processes. As shown in Fig. 9, the poor
322 correlation between pCO_2 and local NCP could be the result of the high pCO_2 water from
323 the Caribbean, which will be discussed in Section 5.2.
324 The multi-year mean sea surface pCO_2 was elevated by 88.0 ppm (from 393.1 to
325 466.5 ppm) for the NGoM Shelf and 56.0 ppm (from 375.1 to 463.1 ppm) for the entire
326 Gulf (Fig. 6, spatially averaged over the sub-regions). This pCO_2 increase was not
327 temporally uniform. On the NGoM Shelf, pCO_2 increases in the no-biology run were
328 clearly higher during spring-summer (with increases of 84.1 and 95.6 ppm) than during
329 fall-winter (with increases of 57.3 and 56.0 ppm). On the Gulf-wide scale, the pCO_2
330 increase was stronger during summer (97.1 ppm) than the other seasons (86.5, 87.6, and
331 80.9 ppm for spring, fall, and winter). For air-sea flux, the elevated surface pCO_2 turns all
332 five sub-regions into a carbon source throughout the year, resulting in a net outflux rate
333 of 2.09 mol C m^{-2} yr^{-1} (Table 1).
334

335 **4.5 Model Sensitivity experiments: historical river forcing (Exp3)**

336 Fig.4 shows that river discharge and DIC inputs during years 1904-1910 as
337 simulated by the DLEM model are comparable with those at present (2004-2010). The
338 multi-year mean value of freshwater discharge is 25,700 m^3/s for 1904-1910 and 23,900
339 m^3/s for 2004-2010. The Mississippi-Atchafalaya delivered 1.51×10^{12} mol C yr^{-1} during
340 1904-1910 and 1.70×10^{12} mol C yr^{-1} during 2004-2010, which is comparable to the
341 increase over the preceding century reported by Raymond et al. (2008), i.e., a 0.24×10^{12}
342 mol C yr^{-1} increase in an average discharge year. However, NO_3 inputs during 1904-1910
343 were < 30% of current inputs (18.12 vs. 63.18×10^9 mol N yr^{-1}). Limited N input led to a
344 smaller primary production not only on the NGoM Shelf, but also the adjacent waters on
345 the WGoM and WF Shelves. Due to the smaller primary production the coastal ocean
346 was a weaker CO_2 sink during spring and summer (Fig. 12) and the NGoM Shelf a year-
347 long carbon source with a net outflux rate of 0.61 mol C m^{-2} yr^{-1} (Table 1). A close
348 examination of the spring and summer conditions on the NGoM Shelf shows that
349 differences in primary production between Exp1 and Exp3 occur mainly along the Texas
350 and Louisiana coasts. Primary production was significantly elevated in the control run
351 because of enhanced NO_3 inputs (Fig. 12a and c). Elevated primary production brought
352 down the sea surface pCO_2. During spring, enhanced primary production and decreased
353 CO_2 was simulated along the Louisiana and Texas coast (Fig. 12b), while during summer,
354 when coastal circulation was influenced by westerly winds, the decreased pCO_2 was
355 more confined within waters along the Louisiana coast.

356

357

5. Discussion

Prior to this investigation, the carbon dynamics in the GoM have been poorly characterized and had a high degree of uncertainty. This study provides one of the first attempts to quantify GoM-wide carbon fluxes and exchanges using a coupled physical-biogeochemical model. We next discuss the factors controlling sea surface pCO_2 variability on the river-influenced NGoM Shelf and the Loop Current-influenced open ocean. The relationship between pCO_2 and other hydrographic variables as well as model uncertainty are also considered.

5.1 NGoM Shelf

The Mississippi-Atchafalaya River and associated plume play the most important role in determining the pCO_2 distribution on the NGoM Shelf. The large input of fluvial DIC and alkalinity introduces carbonate saturation in the coastal waters, conversely, nutrients from the river enhance local primary production, which results in DIC removal and thus reduces sea surface pCO_2 (e.g. Lohrenz et al., 2010; Guo et al., 2012; Huang et al., 2013 and 2015). Such biological removal of CO_2 was also confirmed by the elevated pCO_2 values in the no-biology run in this study. Although the river plume's influence on CO_2 flux has been addressed by prior observational studies, large uncertainties were also found regarding whether the NGoM Shelf is a CO_2 sink or source over a longer time period. For instance, Huang et al. (2013) found a large difference between the pCO_2 distributions in April 2009 and in March 2010. Such a difference was attributed to the variations in river plume extension influenced by local wind conditions and river discharge. In a later communication, based on ship-measurements from 11 cruises, Huang

et al. (2015a) concluded that the NGoM Shelf acted as a net CO_2 sink, but with a large uncertainty (influx rate: 0.96 ±3.7 mol m^{-2} yr^{-1}).

Model results in this study revealed significant spatial and temporal gradients in sea surface pCO_2 as well. The multi-year mean (2005-2010) pCO_2 distribution was characterized by high values in the coastal waters (Fig. 13a), accompanied by low salinity (Fig. 13c), high Dissolved Inorganic Nitrogen (DIN) and high DIC (Figs. 13d and 13e). The pCO_2 value was significantly lower as water became deeper, where the ocean acted as a CO_2 sink during most times of the year (Figs. 7a through d). The surface pCO_2 distribution on the NGoM Shelf was highly correlated with surface salinity (r value: -0.81) and DIN concentration (r value: 0.80) throughout the year, while its correlations with surface temperature and DIC concentration were significant only for part of the year (for detailed season-by-season correlations see Table 2). Although our model suggests that the shelf-wide pCO_2 distribution was positively correlated with DIN concentration, this is not contrary to findings of the above-mentioned observational studies, that is, the high DIN stimulates primary production should be negatively correlated with sea surface pCO_2. Instead, the high DIN concentration, together with the low salinity, was a signal of rich DIC from the riverine inputs and, potentially, the light-limited conditions due to the high suspended sediment and dissolved organic matter concentrations within the river plume. In other words, CO_2 outgassing from oversaturated plume water overwhelmed the CO_2 influx induced by "biological pump" in the areas near the river mouths.

To further link pCO_2 dynamics with biological processes stimulated by river inputs, we plotted the pCO_2 and DIC averaged over spring and summer seasons (high flow from the Mississippi) against surface salinity of the control run and no-biology run

404 in Fig.14. Seawater pCO_2 decreased almost linearly as salinity increased in the no-
405 biology run (Fig. 14b). During spring and summer when river discharge and DIC inputs
406 were high, the high pCO_2 and low salinity waters around the Mississippi River Delta (86-
407 88°W, reddish points) can be easily differentiated from the high salinity and low pCO_2
408 waters on the Texas Shelf (92-95°W, bluish points). The DIC-salinity relationship for
409 waters around the Mississippi Delta (reddish points in Fig. 14d) fell below the
410 conservative mixing relationship for the river end member calculated using in-situ data
411 collected in the spring and summer of 2008 by Cai et al. (2011a). For locations to the
412 west, the DIC-salinity relationship reflected a mixture of waters from the Texas shelf
413 (bluish points) and those from the Atchafalaya river (yellowish-greenish points) likely
414 with differing end members.

415 When biological processes were included, the shelf water exhibited large spatial
416 and seasonal variability (left panels). A pCO_2 minimum was simulated in mid-salinity
417 waters (30-33 psu) during spring and summer, which is consistent with the curve derived
418 by Huang et al., 2015a using ship measurements. Compared with the no-biology run,
419 pCO_2 was reduced significantly and exhibited a wider range in the control run. The
420 biological removal of sea surface CO_2 was most salient in waters around the Mississippi
421 River Delta. The difference in pCO_2 between waters around the delta and the Texas Shelf
422 became more salient. The DIC-salinity relationship for locations around the Mississippi
423 River delta (reddish points in Fig. 14c) indicated a significant carbon removal along the
424 salinity gradient. For waters on the Texas Shelf, the DIC-salinity relationship was
425 confined to higher salinities and slightly increased compared with the no-biology run
426 (bluish points in Fig.14c). The DIC increase on the Texas Shelf in the control run could

427 be linked with the benthic respiration in this region proposed by Hetland and DiMarco
428 (2007).
429
430 **5.2 Open Ocean**
431 In the open ocean, the distribution of surface pCO_2 was strongly related to the
432 surface DIC (r value: 0.93) and alkalinity throughout the year (r value: -0.85, for
433 detailed season-by-season correlations see Table 2). An influence of DIN and primary
434 production was evident in fall and winter months when wind-induced upwelling was
435 strong (Xue et al., 2013). The dependence of pCO_2 on DIC and alkalinity makes the Loop
436 Current an important factor controlling the regional air-sea CO_2 flux. In addition to a
437 relatively high temperature, the Loop Current water is also characterized by low DIC and
438 high alkalinity (Wang et al., 2013 and references therein). The multi-year mean sea
439 surface temperature in Fig.13b shows persistent warm water mass in the form of the Loop
440 Current, which carries the carbonate characteristics of the Caribbean water (i.e. low DIC
441 and high alkalinity, Figs. 13e and 13f). Surface pCO_2 in this warm water mass was
442 significantly lower than surrounding shelf waters (Fig. 13a), making the Loop Current a
443 strong CO_2 sink throughout the year (Figs.7a-d). Any changes in the Caribbean water's
444 carbonate characteristics will affect the carbon budget in the GoM as well as waters
445 further downstream in the Gulf Stream. This is also illustrated by the high pCO_2
446 difference between the control run and no-biology run in Fig. 10 as well as the poor
447 correlation between the pCO_2 drop (difference between control and no-biology runs) and
448 NCP in the Open Ocean (Fig. 11b).
449

5.3 Carbon budget estimation and model uncertainty

Based on our model-simulations, we conclude that the GoM is an overall CO_2 sink, taking up 1.11±0.84 × 10^{12} mol C yr^{-1} from the air. This estimation is comparable to those based on in situ observations, e.g. 1.48 × 10^{12} mol C yr^{-1}, (Coble et al., 2010) and 0.30 × 10^{12} mol C yr^{-1} (Robbins et al. 2014). These recent estimates are in stark contrast to the earlier SOCCR report (Takahashi et al. 2007), which found the GoM to be a CO_2 source (1.58× 10^{12} mol C yr^{-1}, the GoM and Caribbean Sea combined). In addition, we estimated that the GoM received ~ 2.18 × 10^{12} mol C yr^{-1} from rivers, the majority of which was from the Mississippi-Atchafalaya River (~1.80 × 10^{12} mol C yr^{-1}). These two DIC sources (air: ~1.11 × 10^{12} mol C yr^{-1} plus river: ~2.18 × 10^{12} mol C yr^{-1}) largely balance the DIC transported out of the GoM by the Loop Current (~ 3.30 × 10^{12} mol C yr^{-1}, Wang et al., 2013). However, such a balance cannot be achieved using the CO_2 flux estimated by Robbins et al., (2014).

We notice that, during summer months, our model simulated a higher surface pCO_2 than ship measurements on the NGoM Shelf (Fig.6a). As discussed in Section 5.1, a large part of the strong CO_2 degassing was simulated on the Texas Shelf. Yet a close examination of the distribution of available ship measurements indicates that data points on the Texas Shelf are fairly sparse and sporadic (Fig.5), which may partially explain the mismatch between model and ship measurements in Fig.6a. For instance, in the summer of 2010 when more ship measurements were available on the NGoM shelf, both model and observation indicated a high pCO_2 in the summer. In addition, the current model resolution (~5 km) may not be high enough to reproduce small-scale circulation patterns associated with the Mississippi River plume. The complexity of the food web and

uncertainty in model parameterization (e.g. rudimentarily represented denitrification, remineralization, particular organic matters, the lack of phosphate and silicate components, etc.) warrants further investigation.

6. Summary

A coupled physical-biogeochemical model was used to hindcast surface pCO_2 in the GoM from January 2004 to December 2010. Favorable comparisons were found when validating model solutions against ship measurements on the Gulf-wide scale, indicating that this coupled model can reproduce observed pCO_2 variability in the GoM. Time series of spatially averaged pCO_2 for both shelf and open ocean waters exhibit significant seasonal variability, with high values in August and low values in February. Model-simulated pCO_2 values were elevated by 56 and 88 ppm for the entire Gulf and the NGoM shelf, respectively, when the biological sources and sinks of carbon were disabled (i.e., the no-biology run). Without biological processes, the GoM shifts to a strong carbon source with a outflux rate of 2.10 mol C m^{-2} yr^{-1}. Another sensitivity test driven by river conditions from the 1904-1910 period (reduced NO_3 and comparable DIC) indicates the NGoM shelf could have been a CO_2 source with an outflux rate of 0.61 mol C m^{-2} yr^{-1} under those conditions.

The Mississippi-Atchafalaya River plume is the dominant factor controlling the pCO_2 distribution on the NGoM Shelf. Although the NGoM Shelf is overall a CO_2 sink, high surface pCO_2 was simulated in relatively shallow waters, induced by both oversaturated plume water. pCO_2 in the open ocean is controlled largely by the low DIC high alkalinity Loop Current water from the Caribbean Sea.

Our model simulations characterize the GoM as an overall CO_2 sink, taking up ~ $1.11 \pm 0.84 \times 10^{12}$ mol C yr^{-1} from the air. Together with the enormous riverine input (~ 2.18×10^{12} mol C yr^{-1}), this carbon influx was largely balanced by carbon export through the Loop Current estimated by an earlier study. More accurate model predictions of water column DIC concentration will require more in-situ data for improved specification of model DIC initial conditions, and further refinements in model parameterizations to better account for complex carbon dynamics in the coastal ocean.

Acknowledgement

Research support provided through the National Aeronautics and Space Administration (NNX10AU06G, NNX12AP84G, NNX14AO73G, and NNH13ZDA001N); National Science Foundation (OCE-0752254 and OCE-0752110); NOAA Grant NA11NOS0120033; GRI GISR grant SA/GoMRI-006 and GOMRI-020, Fund of China National Programme on Global Change and Air-Sea Interaction (Grant Nos. GASI-GEOGE-03 and GASI-04-01-02); and the National Natural Science Foundation of China (Grant Nos. 41476047 and 41106045) is much appreciated. The operational mode of the SABGOM model is located at http://omgsrv1.meas.ncsu.edu:8080/ocean-circulation/. Data of daily nowcast/forecast model output is hosted at http://omgsrv1.meas.ncsu.edu:8080/thredds/sabgom_catalog.html. Data used in all figures for the hindcast simulation can be obtained by contacting the corresponding author.

519 **References**

520 Aulenbach, B. T., Buxton, H. T., Battaglin, W. T., and Coupe, R. H.: Streamflow and
521 nutrient fluxes of the Mississippi-Atchafalaya River Basin and subbasins for the
522 period of record through 2005: U.S. Geological Survey Open-File Report 2007-1080
523 2007.

524 Bauer, J. E., Cai, W.-J., Raymond, P. A., Bianchi, T. S., Hopkinson, C. S., and Regnier,
525 P. A. G.: The changing carbon cycle of the coastal ocean, Nature, 504, 61-70,
526 10.1038/nature12857, 2013.

527 Benway, H. M., and Coble, P. G.: Introduction. Report of The U.S. Gulf of Mexico
528 Carbon Cycle Synthesis Workshop, Ocean Carbon and Biogeochemistry Program and
529 North American Carbon Program, 63, 2014.

530 Cai, W.-J.: Riverine inorganic carbon flux and rate of biological uptake in the Mississippi
531 River plume, Geophys Res Lett, 30, 1032, 10.1029/2002GL016312, 2003.

532 Cai, W.-J.: Estuarine and Coastal Ocean Carbon Paradox: CO2 Sinks or Sites of
533 Terrestrial Carbon Incineration?, Annual Review of Marine Science, 3, 123-145,
534 doi:10.1146/annurev-marine-120709-142723, 2011a.

535 Cai, W.-J., Hu, X., Huang, W.-J., Murrell, M. C., Lehrter, J. C., Lohrenz, S. E., Chou,
536 W.-C., Zhai, W., Hollibaugh, J. T., Wang, Y., Zhao, P., Guo, X., Gundersen, K., Dai,
537 M., and Gong, G.-C.: Acidification of subsurface coastal waters enhanced by
538 eutrophication, Nature Geosci, 4, 766-770, 2011b.

539 Chassignet, E. P., Hurlburt, H. E., Smedstad, O. M., Halliwell, G. R., Hogan, P. J.,
540 Wallcraft, A. J., Baraille, R., and Bleck, R.: The HYCOM (HYbrid Coordinate Ocean
541 Model) data assimilative system, Journal of Marine Systems, 65, 60-83, 2007.

542 Chavez, F. P., Takahashi, T., Cai, W. J., Friederich, G., Hales, B., Wanninkhof, R., and
543 Feely, R. A.: Coastal Oceans, National Climatic Data Center, Asheville, NC, USA,
544 2007.
545 Coble, P. G., Robbins, L. L., Daly, K. L., Cai, W. J., Fennel, K., and Lohrenz, S. E.: A
546 preliminary carbon budget for the Gulf of Mexico, Ocean Carbon and
547 Biogeochemistry News, 3, 1-4, 2010.
548 Feely, R. A., Sabine, C. L., Lee, K., Berelson, W., Kleypas, J., Fabry, V. J., and Millero,
549 F. J.: Impact of Anthropogenic CO2 on the CaCO3 System in the Oceans, Science,
550 305, 362-366, 10.1126/science.1097329, 2004.
551 Fennel, K.: The role of continental shelves in nitrogen and carbon cycling: Northwestern
552 North Atlantic case study, Ocean Sci, 6, 539-548, 2010.
553 Fennel, K., Hetland, R., Feng, Y., and DiMarco, S.: A coupled physical-biological model
554 of the Northern Gulf of Mexico shelf: model description, validation and analysis of
555 phytoplankton variablity, Biogeosciences, 8, 1881-1899, 2011.
556 Fennel, K., and Wilkin, J.: Quantifying biological carbon export for the northwest North
557 Atlantic continental shelves, Geophys Res Lett, 36, L18605, 10.1029/2009GL039818,
558 2009.
559 Fuentes-Yaco, C., de Leon, D. A. S., Monreal-Gomez, M. A., and Vera-Herrera, F.:
560 Environmental forcing in a tropical estuarine ecosystem: the Palizada River in the
561 southern Gulf of Mexico, Mar Freshwater Res, 52, 735-744, 2001.
562 Gledhill, D. K., Wanninkhof, R., Millero, F. J., and Eakin, M.: Ocean acidification of the
563 Greater Caribbean Region 1996-2006, J Geophys Res-Oceans, C10, 2008.
564 Guo, X., Cai, W.-J., Huang, W.-J., Wang, Y., Chen, F., Murrell, M. C., Lohrenz, S. E.,

565 Jiang, L.-Q., Dai, M., Hartmann, J., Lin, Q., and Culp, R.: Carbon dynamics and
566 community production in the Mississippi River plume, Journal Limnology and
567 Oceanography, 57, 1-17, 2012.
568 Haidvogel, D. B., Arango, H., Budgell, W. P., Cornuelle, B. D., Curchitser, E., Di
569 Lorenzo, E., Fennel, K., Geyer, W. R., Hermann, A. J., Lanerolle, L., Levin, J.,
570 McWilliams, J. C., Miller, A. J., Moore, A. M., Powell, T. M., Shchepetkin, A. F.,
571 Sherwood, C. R., Signell, R. P., Warner, J. C., and Wilkin, J.: Ocean forecasting in
572 terrain-following coordinates: Formulation and skill assessment of the Regional
573 Ocean Modeling System, Journal of Computational Physics, 227, 3595-3624, 2008.
574 Hetland, R., and DiMarco, S.: How does the character of oxygen demand control the
575 structure of hypoxia on the Texas-Louisiana continental shelf?, Journal of Marine
576 Systems, 70, 49-62, 10.1016/j.jmarsys.2007.03.002, 2007.
577 Hofmann, E. E., Cahill, B., Fennel, K., Friedrichs, M. A., Hyde, K., Lee, C., Mannino,
578 A., Najjar, R. G., O'Reilly, J. E., and Wilkin, J.: Modeling the dynamics of
579 continental shelf carbon, Annual review of marine science, 3, 93-122, 2011.
580 Huang, W.-J., Cai, W. J., Castelao, R., Y, W., and Lohrenz, S. E.: Effects of a wind-
581 driven cross-shelf large river plume on biological production and CO2 uptake on the
582 Gulf of Mexico during spring, Limnology and Oceanography, 58, 1727-1735, 2013.
583 Huang, W. J., Cai, W. J., Powell, R. T., Lohrenz, S. E., Wang, Y., Jiang, L. Q., and
584 Hopkinson, C. S.: The stoichiometry of inorganic carbon and nutrient removal in the
585 Mississippi River plume and adjacent continental shelf, Biogeosciences, 9, 2781-
586 2792, 10.5194/bg-9-2781-2012, 2012.
587 Huang, W. J., Cai, W. J., Wang, Y., Lohrenz, S. E., and Murrell, M. C.: The carbon

588 dioxide system on the Mississippi River‐dominated continental shelf in the northern
589 Gulf of Mexico: 1. Distribution and air‐sea CO2 flux, Journal of Geophysical
590 Research: Oceans, 120, 1429-1445, 2015.
591 Lee, K., Wanninkhof, R., Feely, R. A., Millero, F. J., and Peng, T.-H.: Global
592 relationships of total inorganic carbon with temperature and nitrate in surface
593 seawater, Global Biogeochemical Cycles, 14, 979-994, 10.1029/1998GB001087,
594 2000.
595 Mehrbach, C., Culberson, C. H., Hawley, J. E., and Pytkowicx, R. M.: MEASUREMENT
596 OF THE APPARENT DISSOCIATION CONSTANTS OF CARBONIC ACID IN
597 SEAWATER AT ATMOSPHERIC PRESSURE1, Limnology and Oceanography, 18,
598 897-907, 10.4319/lo.1973.18.6.0897, 1973.
599 Millero, F. J.: Thermodynamics of the carbon dioxide system in the oceans, Geochimica
600 et Cosmochimica Acta, 59, 661-677, 1995.
601 Milliman, J. D., and Farnsworth, K. L.: River discharge to the coastal ocean : a global
602 synthesis, Cambridge University Press, Cambridge ; New York, 384 pp., 2011.
603 Murrell, M. C., Stanley, R. S., and Lehrter, J. C.: Plankton community respiration, net
604 ecosystem metabolism, and oxygen dynamics on the Louisiana continental shelf:
605 implications for hypoxia, Continental Shelf Research, 52, 27-38, 2013.
606 Nixon, S. W., Ammerman, J. W., Atkinson, L. P., Berounsky, V. M., Billen, G.,
607 Boicourt, W. C., Boynton, W. R., Church, T. M., Ditoro, D. M., Elmgren, R., Garber,
608 J. H., Giblin, A. E., Jahnke, R. A., Owens, N. J. P., Pilson, M. E. Q., and Seitzinger,
609 S. P.: The fate of nitrogen and phosphorus at the land sea margin of the North
610 Atlantic Ocean, Biogeochemistry, 35, 141-180, 1996.

611 Orr, J. C., Fabry, V. J., Aumont, O., Bopp, L., Doney, S. C., Feely, R. A., Gnanadesikan,
612 A., Gruber, N., Ishida, A., Joos, F., Key, R. M., Lindsay, K., Maier-Reimer, E.,
613 Matear, R., Monfray, P., Mouchet, A., Najjar, R. G., Plattner, G.-K., Rodgers, K. B.,
614 Sabine, C. L., Sarmiento, J. L., Schlitzer, R., Slater, R. D., Totterdell, I. J., Weirig,
615 M.-F., Yamanaka, Y., and Yool, A.: Anthropogenic ocean acidification over the
616 twenty-first century and its impact on calcifying organisms, Nature, 437, 681-686,
617 2005.
618 Rabalais, N., Turner, R. E., and Wiseman, W. J. J.: GULF OF MEXICO HYPOXIA,
619 A.K.A. THE DEAD ZONE, Annual Review of Ecology and Systematics, 33, 235-
620 263, 2002.
621 Raymond, P. A., Oh, N.-H., Turner, R. E., and Broussard, W.: Anthropogenically
622 enhanced fluxes of water and carbon from the Mississippi River, Nature, 451, 449-
623 452, 2008.
624 Robbins, L. L., Wanninkhof, R., Barbero, L., Hu, X., Mitra, S., Yvon-Lewis, S., Cai, W.,
625 Huang, W., and Ryerson, T.: Air-Sea Exchange.Report of The U.S. Gulf of Mexico
626 Carbon Cycle Synthesis Workshop, Ocean Carbon and Biogeochemistry Program and
627 North American Carbon Program, 63, 2014.
628 Sabine, C. L., Feely, R. A., Gruber, N., Key, R. M., Lee, K., Bullister, J. L., Wanninkhof,
629 R., Wong, C. S., Wallace, D. W. R., Tilbrook, B., Millero, F. J., Peng, T. H., Kozyr,
630 A., Ono, T., and Rios, A. F.: The oceanic sink for anthropogenic CO2, Science, 305,
631 367-371, 2004.
632 Sabine, C. L., and Tanhua, T.: Estimation of Anthropogenic CO2 Inventories in the
633 Ocean, Annual Review of Marine Science, 2, 175-198, doi:10.1146/annurev-marine-

120308-080947, 2010.

Shchepetkin, A. F., and McWilliams, J. C.: The Regional Ocean Modeling System (ROMS): a split-explicit, free-surface, topography-following coordinates ocean model, Ocean Modelling, 9, 347-404, 2005.

Stocker, T., Qin, D., Plattner, G.-K., Tignor, M., Allen, S. K., Boschung, J., Nauels, A., Xia, Y., Bex, V., and Midgley, P. M.: Climate change 2013: The physical science basis, Cambridge University Press Cambridge, UK, and New York, 2014.

Sturges, W., and Leben, R.: Frequency of Ring Separations from the Loop Current in the Gulf of Mexico: A Revised Estimate, Journal of Physical Oceanography, 30, 1814-1819, 2000.

Takahashi, T., Sutherland, S. C., and Kozyr, A.: Global Ocean Surface Water Partial Pressure of CO2 Database: Measurements Performed During 1957-2012 (Version 2014), Carbon Dioxide Information Analysis Center, Oak Ridge National Laboratory, U.S. Department of Energy, Oak Ridge, Tennessee, 2015.

Tian, H., Ren, W., Yang, J., Tao, B., Cai, W.-J., Lohrenz, S., Hopkinson, C., Liu, M., Yang, Q., Lu, C., Zhang, B., Banger, K., Pan, S., He, R., and Xue, Z.: Climate extremes dominate seasonal and interannual variations in carbon export from the Mississippi River Basin, Global Biogeochemical Cycles, 29, 10.1002/2014GB005068, 2015.

Tsunogai, S., Watanabe, S., and Sato, T.: Is there a "continental shelf pump" for the absorption of atmospheric CO2?, Tellus B, 51, 701-712, 1999.

Uppström, L. R.: The boron/chlorinity ratio of deep-sea water from the Pacific Ocean, Deep Sea Research and Oceanographic Abstracts, 1974, 161-162,

Wang, Z. A., Wanninkhof, R., Cai, W.-J., Byrne, R. H., Hu, X., Peng, T.-H., and Huang, W.-J.: The marine inorganic carbon system along the Gulf of Mexico and Atlantic coasts of the United States: Insights from a transregional coastal carbon study, Limnology and Oceanography, 58, 325-342, 2013.

Weiss, R. F.: Carbon dioxide in water and seawater: the solubility of a non-ideal gas, Marine Chemistry, 2, 203-215, 1974.

Weiss, R. F., and Price, B. A.: Nitrous oxide solubility in water and seawater, Marine Chemistry, 8, 347-359, 1980.

Xue, Z., He, R., Fennel, K., Cai, W., Lohrenz, S., and Hopkinson, C.: Modeling Seasonal and Interannual Variability of Circulation and Biogeochemical Processes in the Gulf of Mexico, Biogeosciences, 10, 7219-7234, 2013.

Xue, Z., Zambon, J., Yao, Z., Liu, Y., and He, R.: An Integrated Ocean Circulation, Wave, Atmosphere and Marine Ecosystem Prediction System for the South Atlantic Bight and Gulf of Mexico, Journal of Operational Oceanography, 8, 2015.

Zeebe, R., and Wolf-Gladrow, D.: CO2 in Seawater: Equilibrium, Kinetics, Isotopes, Elsevier, Amsterdam, 2001.

Tables and Figures

Table 1. Comparison between observed and modeled air-sea CO_2 flux. Observations are taken from Robins et al (2014), whereas the model results are seven-year (2005-2010) model mean*.

		Sub-regions					
		Mexico Shelf	**Western Gulf**	**Northern Gulf**	**West Florida Shelf**	**Open Ocean**	**Gulf-wide****
Subregion Area (10^{12} m^2)		0.18	0.08	0.15	0.15	1.01	1.56
Simulation 1 (control run)*	Spring	0.97±0.29	-0.24±0.59	1.01±0.89	0.28±0.33	1.51±0.41	1.23±0.48
	Summer	-0.96±0.38	-1.69±0.43	-1.42±0.74	-1.26±0.53	-0.33±0.33	-0.62±0.52
	Fall	-0.76±0.45	-1.06±0.34	-0.79±0.63	-1.73±0.67	0.56±0.61	0.06±0.66
	Winter	0.49±0.28	1.62±0.32	2.49±0.70	1.19±0.38	2.44±0.49	2.21±0.40
	Annual	**0.19±0.35**	**-0.34±0.42**	**0.32±0.74**	**-0.38±0.48**	**1.04±0.46**	**0.71±0.54**
Robbins et al., 2014	**Annual**	**0.09±0.05**	**-0.18±0.05**	**0.44±0.37**	**-0.37±0.11**	**0.48±0.07**	**0.19±0.08**
Simulation 2 (no-bio)	Annual	-2.77±0.36	-2.02±0.36	-1.64±0.68	-1.79±0.36	-2.08±0.39	-2.10±0.46
Simulation 3 1904-1910	Annual	0.08±0.35	-0.77±0.77	0.61±1.07	0.55±0.46	0.86±0.46	0.50±0.65

*unit: mol m^{-2} yr^{-1}, + indicates ocean is an air CO_2 sink; - indicates a CO_2 source to the atmosphere

**Gulf-wide value is a sum of all sub-regions.

682 Table 2. Spatial correlation coefficients between pCO_2, sea surface temperature (SST),
683 sea surface salinity (SSS), dissolved inorganic nitrate (DIN: NO_3+NH_4), dissolved
684 inorganic carbon (DIC), alkalinity (ALK), and primary production (P-Prod) on the
685 Louisiana Shelf and in the open ocean (multi-year mean of 2005-2010, control run).

Correlation Coefficient (R value)		**SST**	**SSS**	**DIC**	**DIN**	**ALK**	**P-Prod**
pCO_2 on the NGoM	Spring	-0.24	**-0.81**	-0.12	**0.86**	-0.77	0.36
	Summer	0.63	**-0.65**	0.65	**0.66**	-0.17	0.35
	Fall	-0.66	**-0.87**	0.86	**0.78**	0.17	0.58
	Winter	-0.67	**-0.89**	0.45	**0.89**	-0.90	0.23
	Annual	-0.64	**-0.82**	0.63	**0.82**	-0.65	0.47
pCO_2 in open ocean	Spring	0.11	0.17	**0.76**	-0.27	**-0.70**	-0.41
	Summer	-0.11	-0.11	**0.99**	-0.29	**-0.91**	-0.43
	Fall	0.04	0.08	**0.96**	-0.77	**-0.88**	-0.76
	Winter	0.04	-0.05	**0.75**	-0.49	**-0.69**	-0.55
	Annual	-0.17	0.05	**0.93**	-0.50	**-0.85**	-0.59

686

687

688

689 Figure 1. Domain of the South Atlantic Bight and Gulf of Mexico (SABGOM) ROMS
690 model with water depth in color (unit: m). Also shown are the five sub-regions used in
691 this study, which are Mexico Shelf (MX), Western Gulf of Mexico Shelf (WGoM),
692 Northern Gulf of Mexico Shelf (NGoM), West Florida Shelf (WF), and open ocean. Also
693 shown is a schematic for the Loop Current.
694

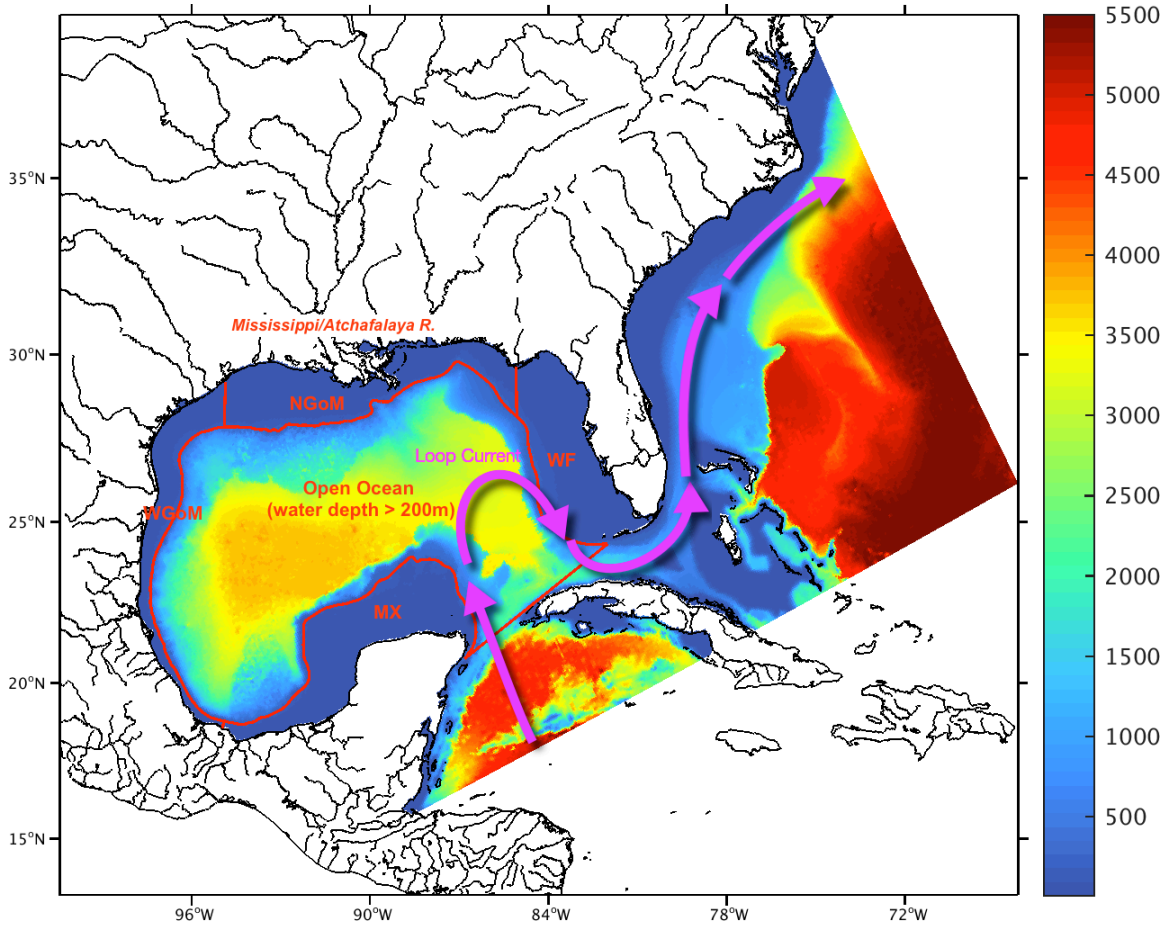

695

Figure 2. DIC and alkalinity initial conditions derived from the empirical relationship by Lee et al. (2000 and 2006).

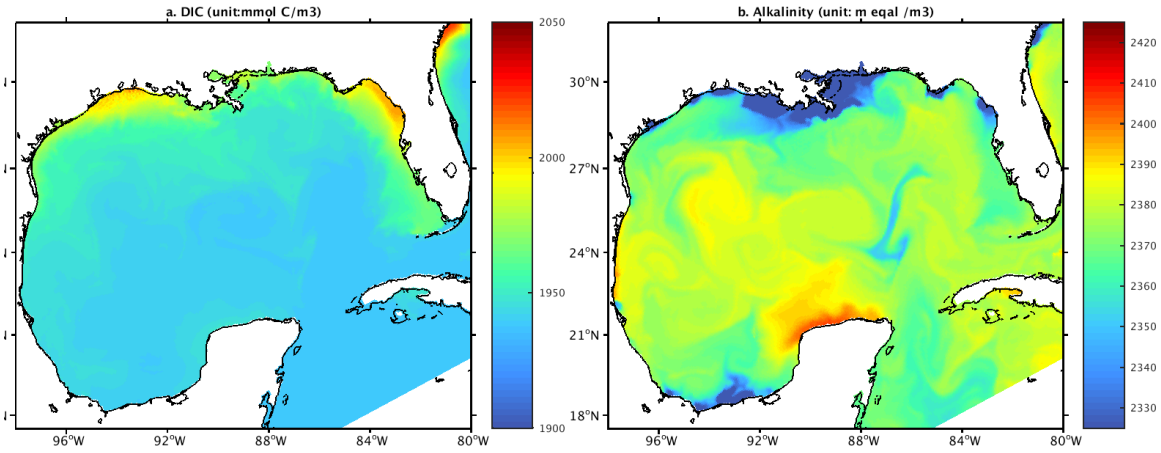

Figure 3. Satellite observed monthly pCO_2 (AIRS) averaged over the Gulf of Mexico (red stars) and the pCO_2 air used in model air-sea CO_2 flux calculation (blue line), which is generated using the curve-fitting software CCGCRV.

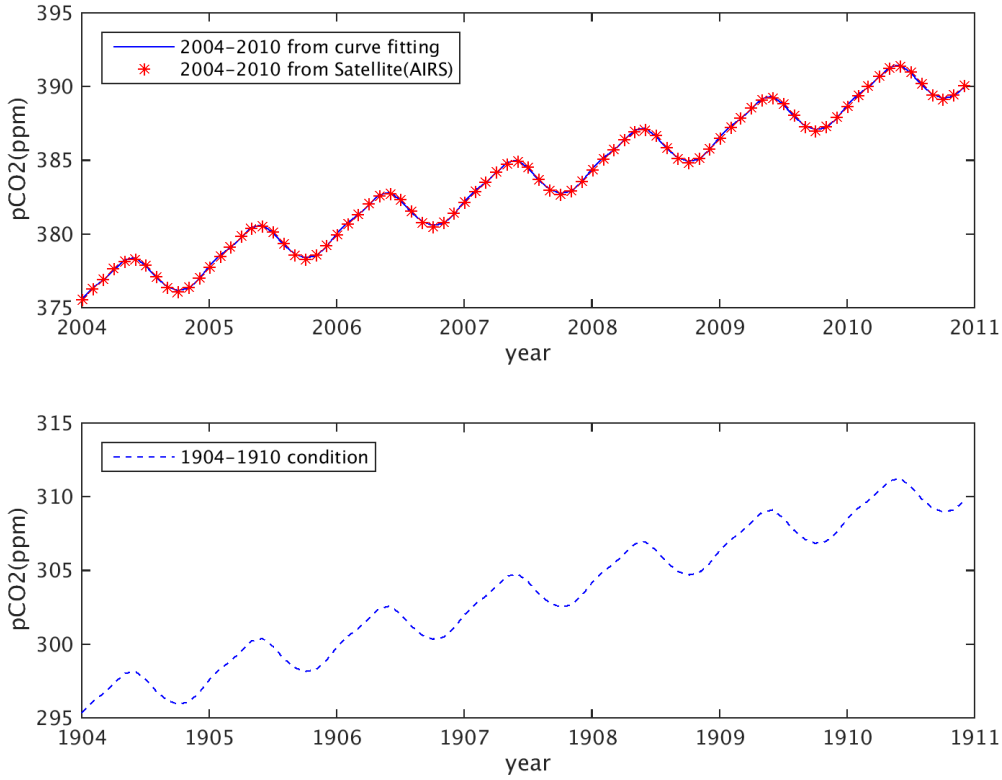

704 Figure 4. Comparisons between the 2005-2010 riverine DIC and NO_3 conditions
705 observed by USGS (red line) and the 1904-1910 river condition simulated by the
706 Dynamic Land Ecosystem Model (black line, Tian et al., 2015).
707

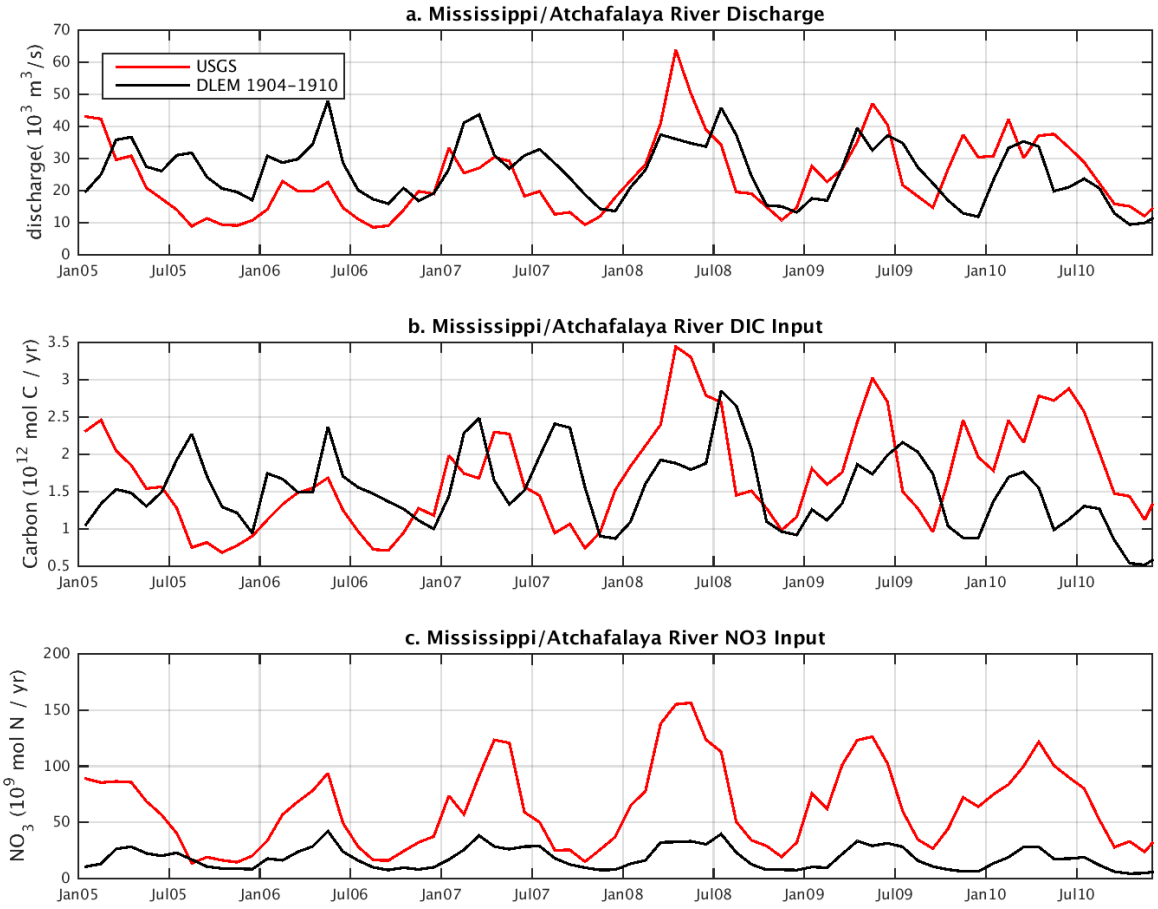

708

709 Figure 5. Locations of in-situ measurements from the LDEO database (blue) and Huang

710 et al. (2015, grey) in the period of 2005-2010.

711

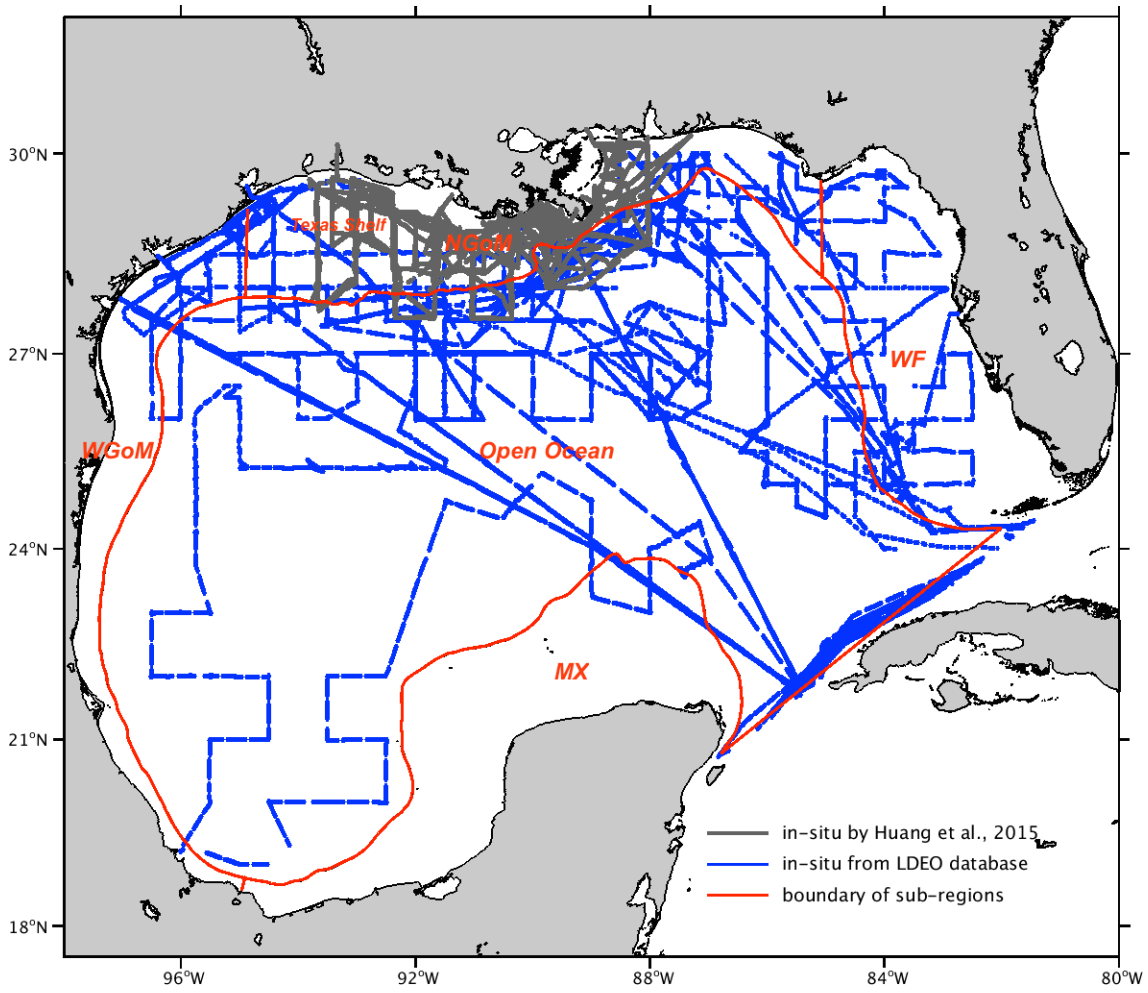

712

Figure 6. Time series of spatially averaged pCO_2 (control run in blue and no-biology run in red) (a) on the Northern Gulf of Mexico shelf, and (b) in the entire Gulf of Mexico, overlaid with in situ observations (in black) from Huang et al. (2015a and b), and Takahashi et al. (2015).

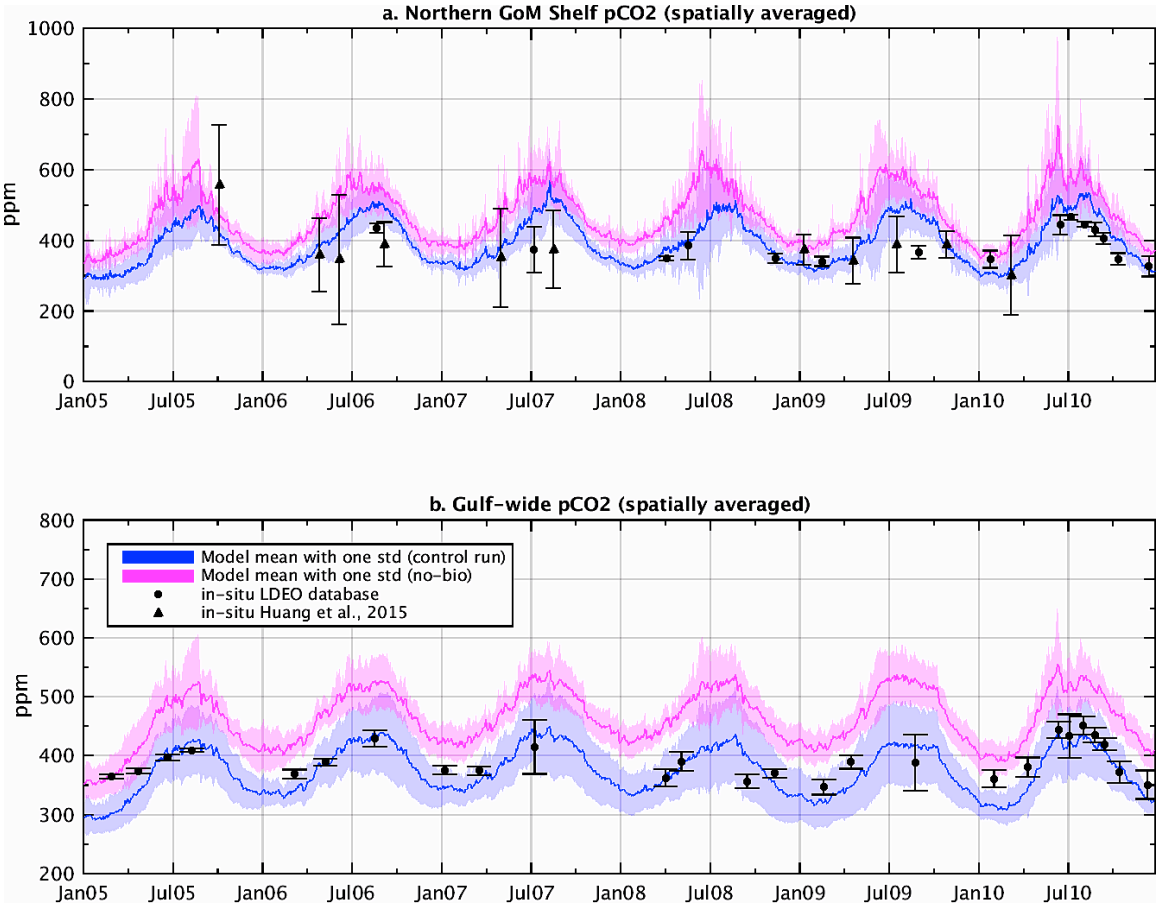

719 Figure 7. Six-year (2005-2010) model (control run) mean air-sea CO_2 flux in the Gulf of
720 Mexico during (a) spring, (b) summer, (c) fall, and (d) winter. Blue color indicates where
721 the ocean is a sink for CO_2; red color indicates where the ocean is a source.
722

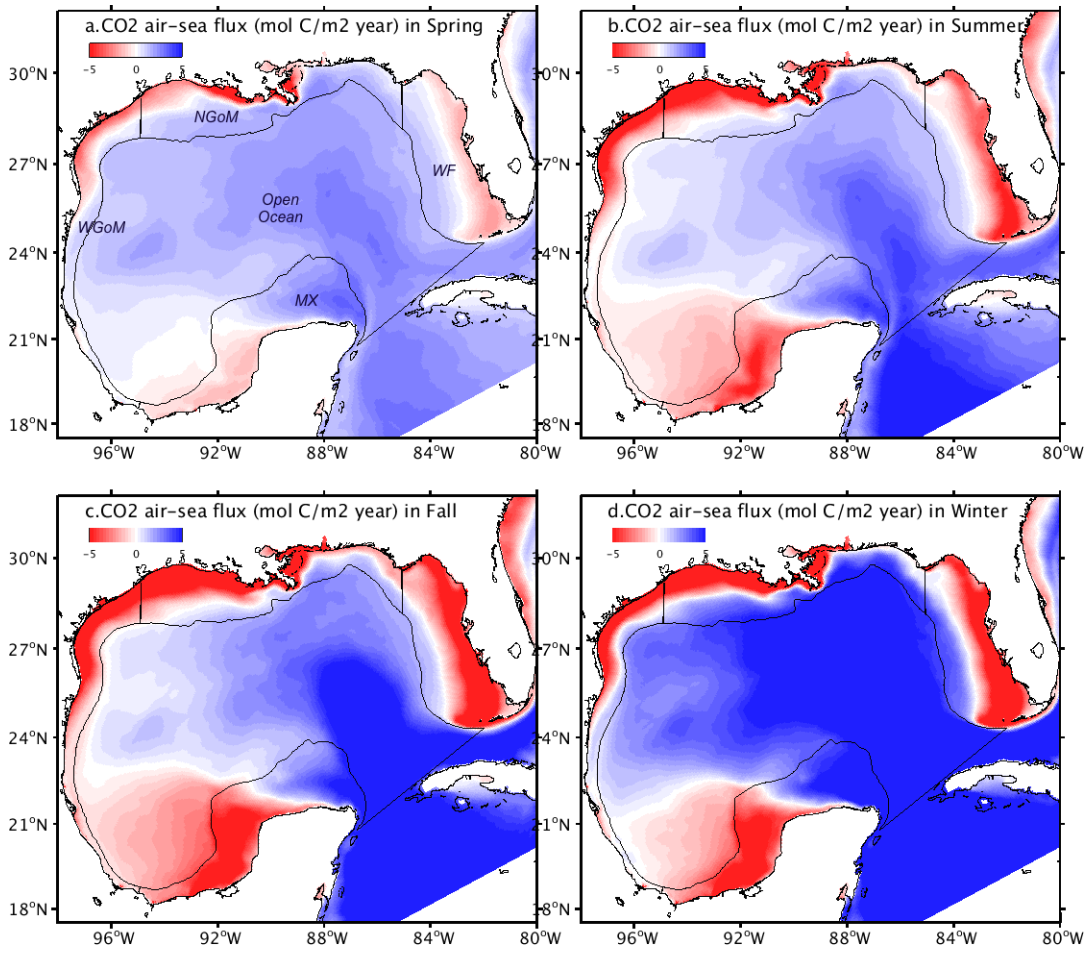

723

724 Figure 8. Six-year (2005-2010) model (control run) mean surface Net Community
725 Production (NCP) in the Gulf of Mexico during (a) spring, (b) summer, (c) fall, and (d)
726 winter.

727
728

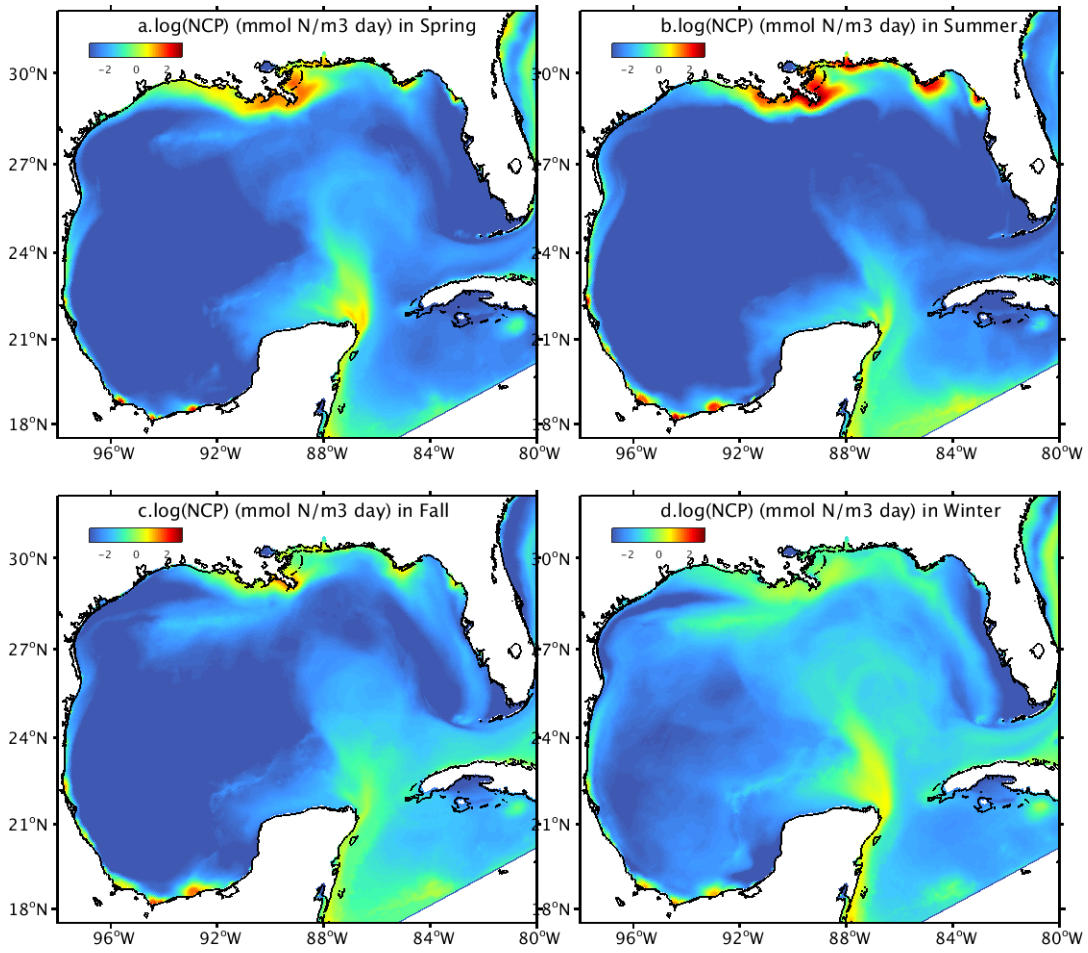

729

730 Figure 9. Time series of spatially averaged Net Community Production (a) on the
731 Northern Gulf of Mexico shelf, and (b) in the entire Gulf of Mexico (unit: mmol N/m^3).
732

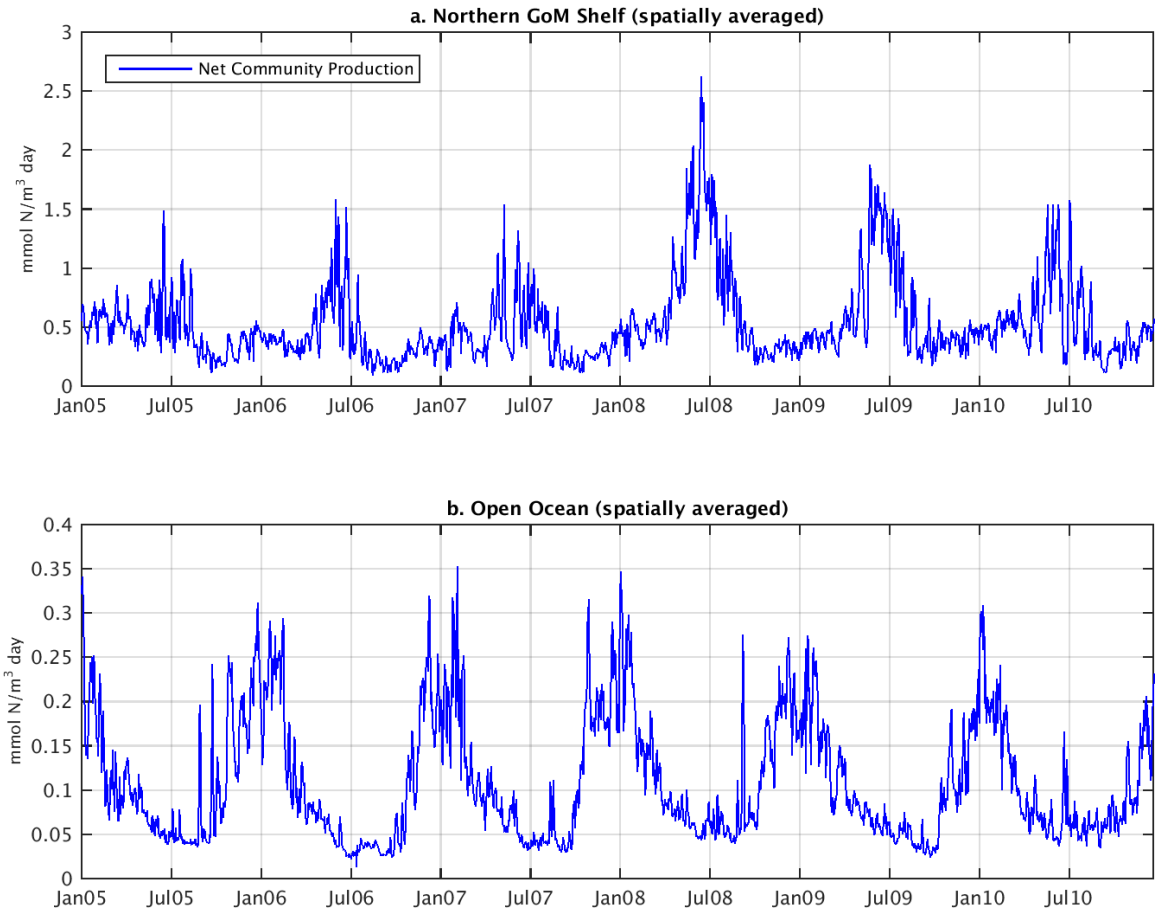

733
734
735

736 Figure 10. Multiyear (2005-2010) seasonal mean pCO_2 elevation (No-biology run minus

737 control run, in the Gulf of Mexico during (a) spring, (b) summer, (c) fall, and (d) winter.

738

739

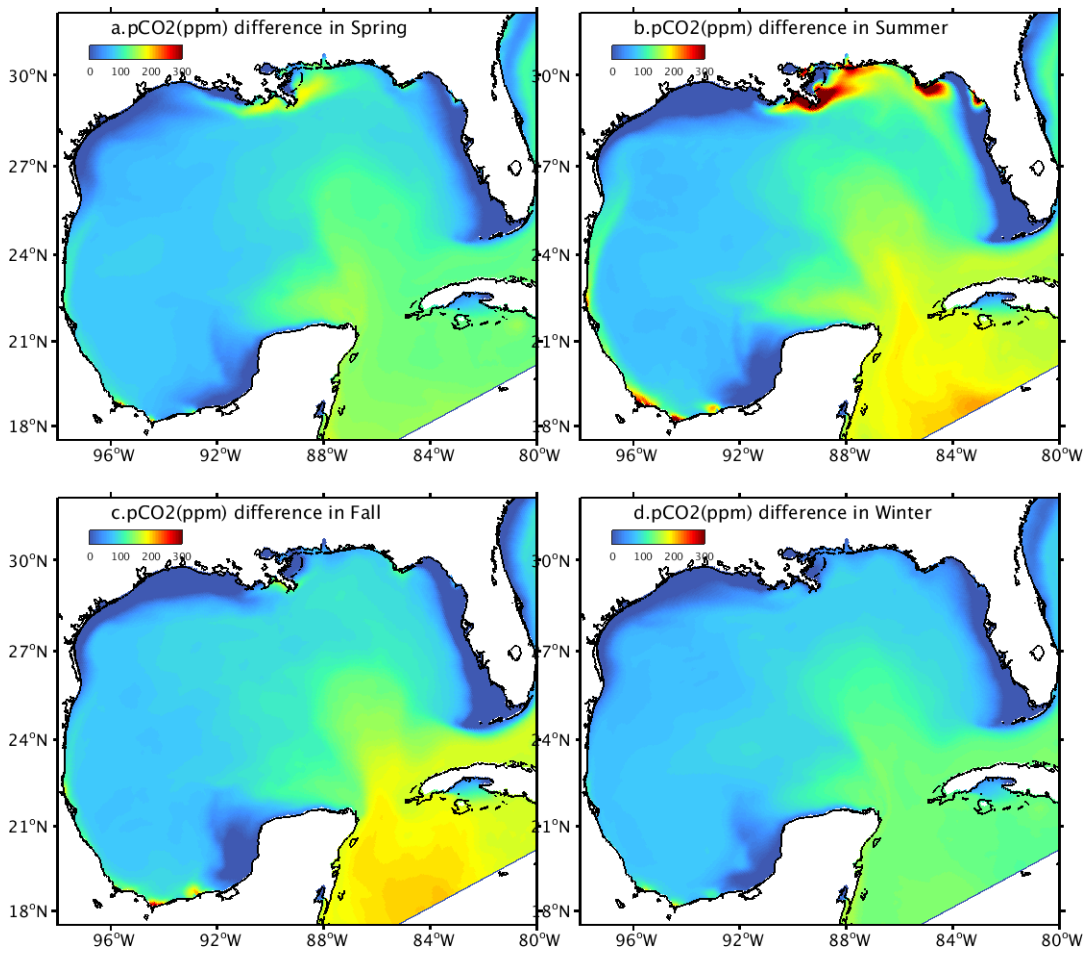

740

741 Figure 11. Scatter plots of the multiyear mean pCO_2 drop (No-biology run minus Control

742 run) and surface NCP in NGoM (left) and Open Ocean (right).

743
744

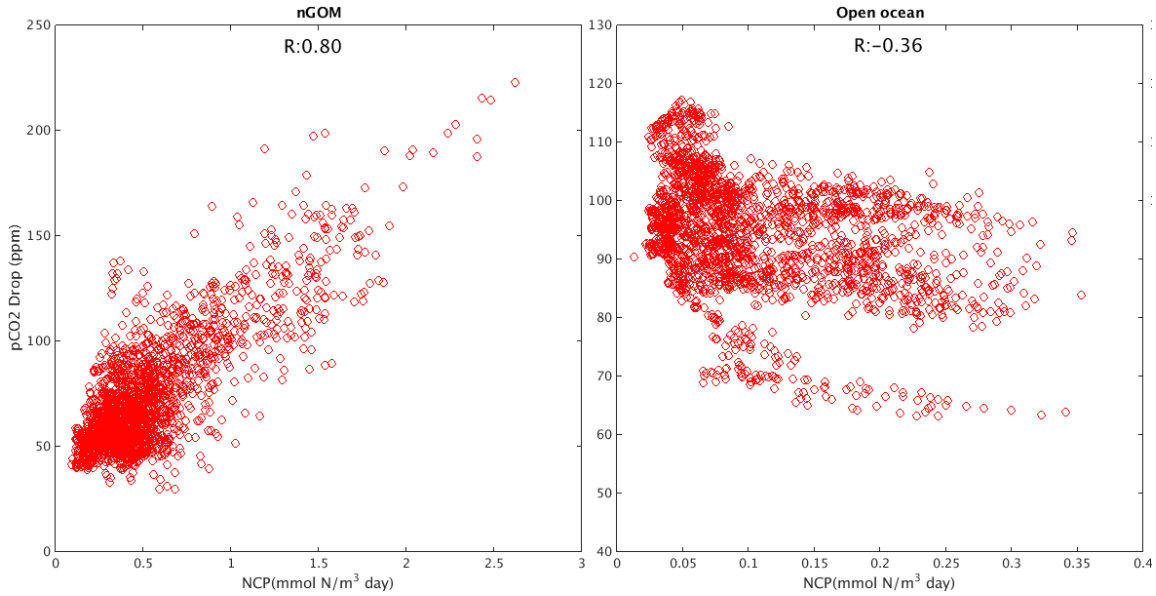

745
746
747

748 Figure 12. Differences in model simulated primary production and pCO_2 between the
749 2004-2010 and the 1904-1910 periods (2005-2010 minus 1905-1910 seasonal mean
750 condition). For a) and c) blue color indicates increased primary production during 2004-
751 2010, for b) and d) red color indicates reduced pCO_2 during 2004-2010.

752

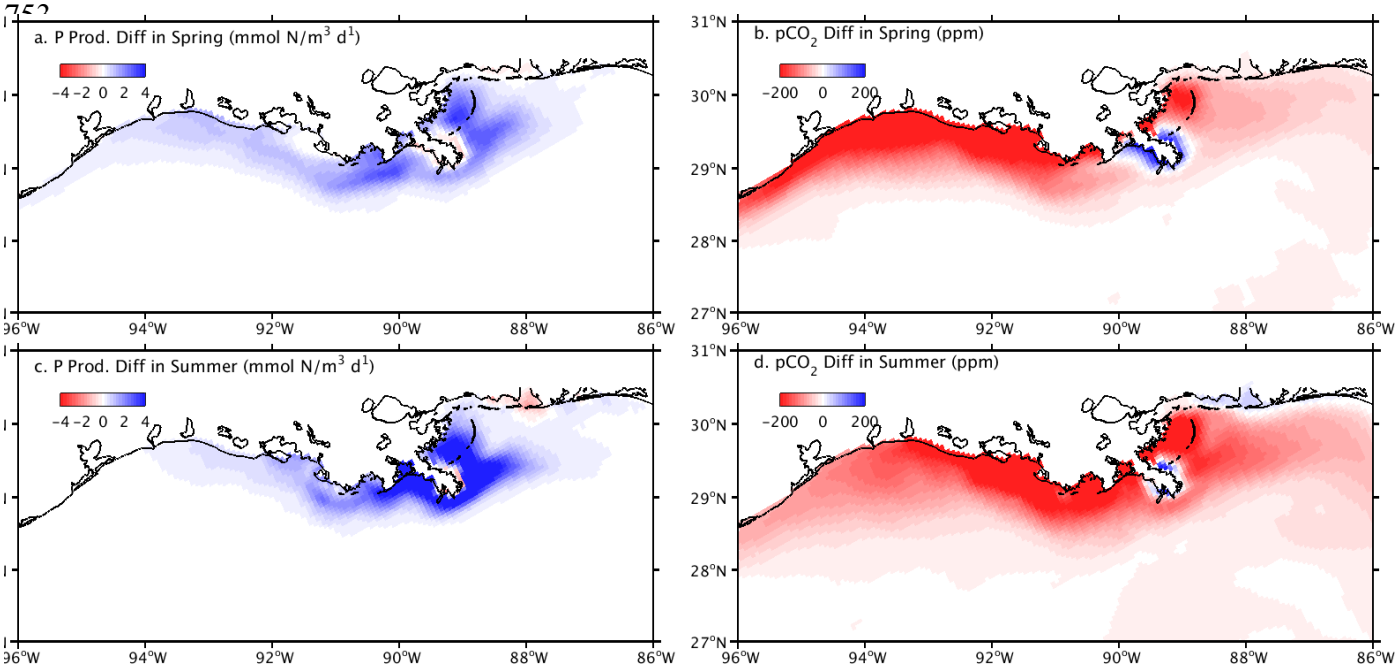

754 Figure 13. Six-year mean (2005-2010) surface conditions simulated by the model for a)
755 pCO_2 (ppm), b) temperature (degree C), c) salinity, d) dissolved inorganic carbon (mmol
756 C m^{-3}), e) dissolved inorganic nitrogen (NO_3+NH_4) (mmol N m^{-3}), and f) alkalinity (mEq
757 m^{-3}).
758
759 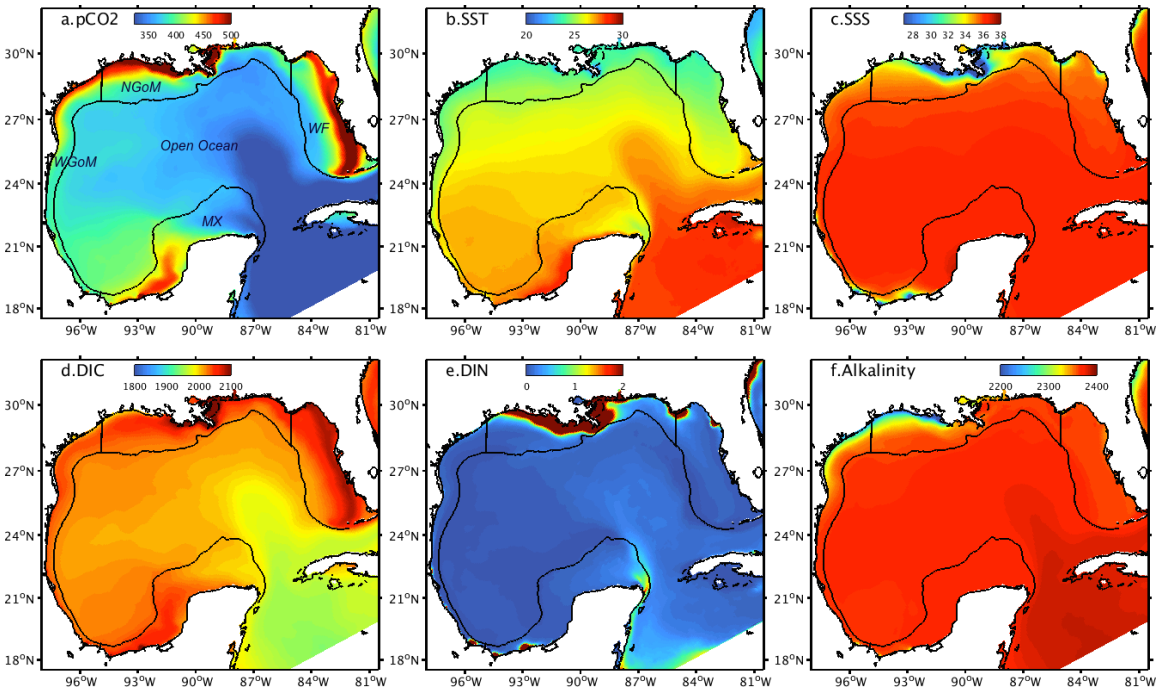

760
761
762

Figure 14. Six-year (2005-2010) spring-summer mean condition of model simulated sea surface pCO_2 and DIC against salinity for the control run (a and c) and no-biology run (b and d) on the NGoM Shelf; also shown are longitude with colors (note that the Mississippi river delta is located around 89°W and Atchafalaya river delta is located around 91°W). Also shown in c) and d) are conservative mixing relationships for river end members from Cai et al. (2011a).

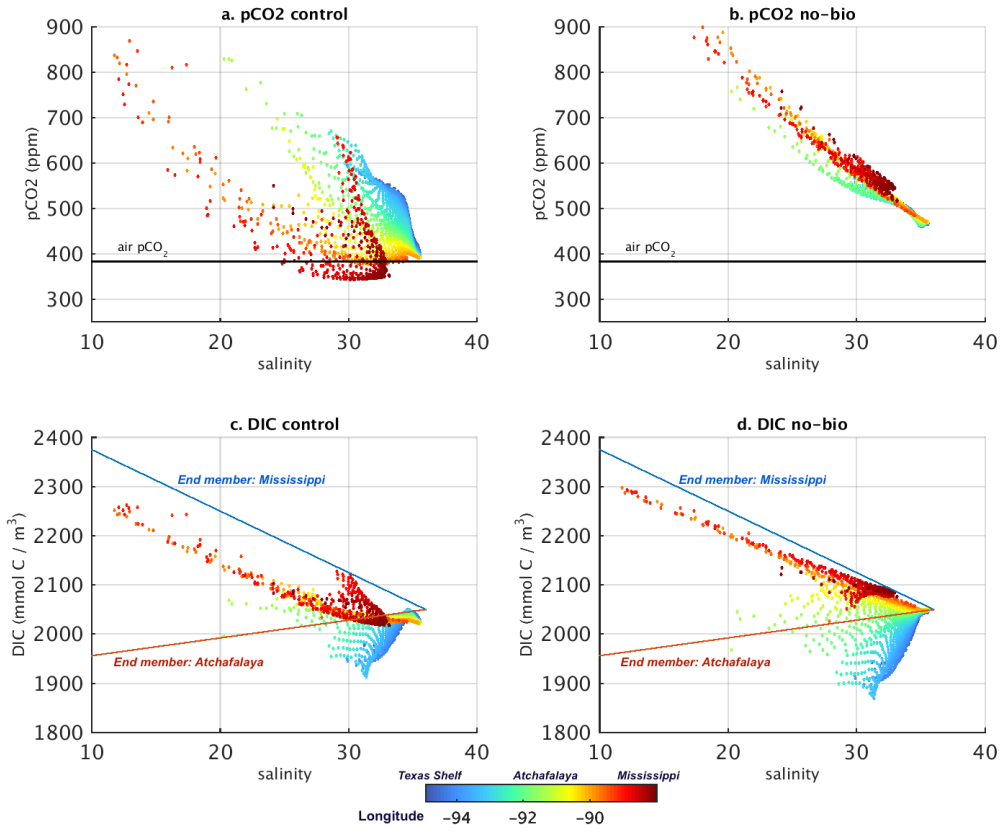

Supplementary Materials

S1. Calculation of seawater pCO_2

The seawater pCO_2 was calculated following Zeebe and Wolf-Gladrow (2001) as follows:

$$pCO_2=DIC*[H^+]^2/([H^+]^2+K_1*[H^+]+K_1*K_2)/f \quad (1)$$

where DIC is the dissolved inorganic carbon and was given by model input. K_1 and K_2 are constant of carbonic acid, $K_1=[H^+]*[HCO_3^-]/[H_2CO_3]$, $K_2=[H^+]*[CO_3^{2-}]/[HCO_3]$ and were calculated following Millero (1995) using data from Mehrbach et al. (1973) as follows:

$$logK_1=62.008-1/T*3670.7-logT*9.7944+S*(0.0118-S*0.000116) \quad (2)$$

$$logK_2=-4.777-1/T*1394.7-logT*9.7944+S*(0.0184-S*0.000118) \quad (3)$$

where in (2) and (3) the T is for water temperature (unit: K) and S is for salinity;

The f in (1) is the correction term for non-ideality and was calculated from Weiss and Price (1980) using equation 13 with 6 values. $[H^+]$ is solved using the 5th order polynomial bracket and bisection method with the following 5 coefficients:

$$p5=1; \quad (4)$$

$$p4=-Alk-K_b-K_1; \quad (5)$$

$$p3=DIC*K_1-Alk*(K_b+K_1)+K_b*borate+K_w-K_b*K_1-K_1*K_2; \quad (6)$$

$$p2=DIC*(K_b*K_1+2*K_1*K_2)-Alk*(K_b*K_1+K_1*K_2)+$$

$$K_b*borate*K_1+(K_w*K_b+K_w*K_1-K_b*K_1*K_2); \quad (7)$$

$$p1=2*DIC*K_b*K_1*K_2-Alk*K_b*K_1*K_2+K_b*borate*K_1*K_2+K_w*K_b*K_1+K_w*K_1*K_2; \quad (8)$$

$$p0=K_w*K_b*K_1*K_2; \quad (9)$$

where *Alk* is for total alkalinity (unit: milli-equivalent per liter) and was given by model input; K_w is ion product of water ($[H^+]*[OH^-]$) and K_b is the constant of boric acid ($[H^+]*[BO_2^-]/[HBO_2]$), which were calculated following Millero (1995):

$$lnK_b=-8966.90+2890.51*S^{0.5}-77.942*S+1.726*S^{1.5}-0.0993*S^2)/T+(148.0248+137.194*S^{0.5}+1.62247*S+(-24.4344-25.085*S^{0.5}-0.2474*S)*lnT+0.053105*S^{0.5}*T) \quad (10)$$

$$lnK_w=148.9802-13847.26/T-23.6521*lnT+(-0.977+118.67/T+1.0495*lnT)*S^{0.5}-0.01615*S) \quad (11)$$

and borate stands for the concentrations for borate and was calculated following Uppstrom (1974):

$$borate=0.000232*S/1.80655/10.811 \quad (12)$$

S2. Model initial and boundary condition setup for Dissolved Inorganic Carbon (DIC) and alkalinity

The initial and boundary conditions for DIC follow the relationship between DIC and Sea Surface Temperature (SST) for the western (sub)tropical Atlantic waters described in Lee et al., 2000 as follows:

$$DIC=1940+1.842*(SST-29)+0.468*(SST-29)^2 \quad (13)$$

For alkalinity, we use the relationship among DIC and SST and Sea Surface Salinity (SSS) for the sub(tropical) waters described in Lee et al., 2006 as follows:

$$Alkalinity= 2305+58.66*(SSS-35)+2.32*(SSS-35)*(SSS-35)-1.41*(SST-20)+0.040*(SST-20)*(SST-20); \quad (14)$$

S3. Air-Sea CO_2 flux calculation

The air-sea CO2 flux was calculated following Wanninkhof (1992) as follows:

$$F=K*(pCO_{2\ air}- pCO_{2\ water}) \quad (15)$$

where pCO_2 air is the air pCO_2, and $pCO_{2\ water}$ was calculated from (1); F is the air-sea CO_2 flux (unit: millimole C meter^{-2} day^{-1});

$$K=kL \quad (16)$$

where L is the solubility of CO_2 and was calculated following Weiss (1974) as follows:

$$ln\ L= -60.2409+93.4517/T+23.3585*Log(T) +S*(0.023517+T*(-0.023656+0.0047036*T)) \quad (17)$$

and the k in (14) is the gas transfer velocity and was calculated using

$$k=0.31u^2(Sc/660)^{-0.5} \quad (18)$$

where u is the wind speed at 10 m above sea-level from the North America Regional Reanalysis dataset; Sc is the Schmidt number and was set to

$$Sc=2073.1-125.62*T+36276*T^2-0.043219*T^3 \quad (19)$$